Combined analysis of electricity and heat networks ✩

Xuezhi Liu [a], Jianzhong Wu [a,*], Nick Jenkins [a], Audrius Bagdanavicius [b]

[a] Institute of Energy, Cardiff University, Queen's Buildings, The Parade, Cardiff CF24 3AA, UK
[b] Department of Engineering, University of Leicester, University Road, Leicester LE1 7RH, UK

HIGHLIGHTS

- Analysis of district heating networks was performed by the hydraulic-thermal model.
- Electricity and heat networks were investigated as a whole by combined analysis.
- The integrated method required less iteration than the decomposed method.
- An engineering solution was provided to a case study of Barry Island.

ARTICLE INFO

ABSTRACT

Energy supply systems are usually considered as individual sub-systems with separate energy vectors. However, the use of Combined Heat and Power (CHP) units, heat pumps and electric boilers creates linkages between electricity and heat networks. Two combined analysis methods were developed to investigate the performance of electricity and heat networks as an integrated whole. These two methods were the decomposed and integrated electrical-hydraulic-thermal calculation techniques in the forms of power flow and simple optimal dispatch. Both methods were based on models of the electrical network, hydraulic and thermal circuits, and the coupling components, focusing on CHP units and circulation pumps. A case study of Barry Island electricity and district heating networks was conducted, showing how both electrical and heat demand in a self-sufficient system (no interconnection with external systems) were met using CHP units. The comparison showed that the integrated method requires less iteration than the decomposed method.

© 2015 Published by Elsevier Ltd.

1. Introduction

Energy supply systems are usually considered as individual sub-systems with separate energy vectors, e.g. electricity, heat, gas or hydrogen. In the present Smart Grid vision [1], the role of electricity is most prominent with limited consideration of other energy networks. However, there are many benefits to be gained by considering the energy system as an integrated whole. Energy flows supplied from alternative sources can be controlled; therefore, security of energy supply could be increased. The most energy efficient operating regime can be determined and energy losses, costs and emissions could be minimised. Independent planning and operation of separate energy networks will unlikely yield an overall optimum, since synergies between the different energy vectors cannot be exploited. Thus, an integration of energy systems is highly desirable [2,3].

One of the examples of integrated energy networks is district heating systems with Combined Heat and Power (CHP) units. CHP units, electric boilers and heat pumps connected to a district heating system act as linkages between electricity and heat networks. Such integrated electricity and heat networks with energy storage could contribute to more efficient utilisation of distributed energy [4,5]. The coupling components (CHP units, heat pumps, electric boilers and circulation pumps) increase the flexibility for equalising the fluctuations from the renewable energy. As the penetration of the renewable energy sources increases [6], the interaction of electricity and heat networks becomes tighter and modelling of electricity and heat networks as a whole becomes more important.

Several approaches for modelling the integration of different energy systems have been published. Examples include energy hubs [2], multi-energy systems and distributed multi-generation [5,7–9], intelligent energy systems [10], community energy [7], smart energy systems [11], and integrated energy systems [12].

A generic framework for steady-state analysis and optimisation of energy systems was investigated by Geidl and Andersson [2]. The coupling between multiple energy carriers was modelled using energy hubs. Using the energy hubs concept, input power of electricity, natural gas and district heat is converted to electricity and heat output power through an efficiency coupling matrix. The model showed the potential for reduction of overall energy cost and emissions.

Smart multi-energy and distributed multi-generation systems were described by Mancarella et al. [7–9]. In multi-energy systems, coupling of electricity, heating, cooling and gas networks takes place through various distributed technologies such as CHP, micro-CHP, heat pumps, solar thermal, photovoltaic and energy storage systems. A holistic overview from an energy, environmental, and techno-economic perspective was provided.

Several methods were developed to investigate combined electricity and natural gas networks [2,13–18], where gas turbine generators are the linkages between the gas and electricity networks. An approach was used to execute a single gas and power flow analysis in a unified framework based on the Newton–Raphson formulation [17].

A few studies investigated the combined electricity and heat networks, e.g. an integrated optimal power flow of electricity and heat networks [19]. On the other hand, several studies investigated the coupling components within combined electricity and heat networks. The impact of heat pumps and distributed CHP on low voltage networks was evaluated by Mancarella et al. [20], showing how a smart combination of these technologies could reduce the arising network impact (particularly severe in the case of heat pumps [21]). Technology options such as electric boilers and heat pumps that allow for distributed CHP to better co-exist with intermittent renewables were investigated [22]. In these studies, detailed analysis of heat networks was not conducted. The integration of technical design, greenhouse gas emission analysis and financial analysis for integrated community energy systems was modelled by Rees et al. [23–25]. In these models the electrical, thermal and gas power flows were calculated independently and linked through generating units.

Two methods for combined analysis were developed to investigate the performance of electricity and heat networks. The methods were based on the hydraulic-thermal model of heat networks and the electrical power flow model. The decomposed analysis method is to solve the independent hydraulic equations, thermal equations, and electrical power flow equations sequentially. The integrated analysis method is to solve the combined hydraulic equations and thermal equations, and electrical power flow equations simultaneously as an integrated whole. In this paper the description of both methods and the results of analysis using a case study were presented.

2. Combined electricity and district heating networks

A schematic drawing of combined electricity and district heating networks is shown in Fig. 1. The electricity and heat networks are linked through the coupling components (e.g., CHP units, heat pumps, electric boilers and circulation pumps), which are represented as the Sources in Fig. 1. These coupling components allow the flows of energy between the two networks. CHP units generate electricity and heat simultaneously; heat pumps and electric boilers convert electricity to heat; circulation pumps consume electricity to circulate water in the district heating network. These coupling components increase the flexibility of the electricity and heat supply systems for facilitating the integration of intermittent renewable energy.

From the modelling point of view, heat pumps or electric boilers are equivalent to CHP units with negative electrical power output. Electrical power generators are equivalent to CHP units with zero heat output. These components are generalised as an electrical and heat interface with adjustable heat-to-power ratio. Heat and electrical power outputs of the interface are described by their equivalent heat-to-power ratios as introduced by Mancarella [26].

Conventional electrical power flow calculations use a single slack busbar. While in the integrated analysis of the combined networks, one electrical slack busbar and one heat slack node are used.

In the case of islanded operation of the electrical network, two CHP units are chosen as the slack node and the slack busbar (Source 1 and Source 2 in Fig. 1). In grid-connected mode as shown in Fig. 2, the electricity slack busbar is chosen as the grid connection point, so there is no heat generated at the electricity slack busbar. Therefore, the grid-connected mode can be considered as a simplified special case of islanded operation.

Other than the CHP unit being the electricity slack busbar, CHP units with adjustable real power output and voltage magnitude are classified as PV busbars; the other CHP units such as micro-CHP are classified as PQ busbars with given real and reactive power output.

CHP units and other coupling components allow flows of energy between the two networks. In islanded mode, the heat power generated by Source 2 (at the electricity slack busbar) is determined by
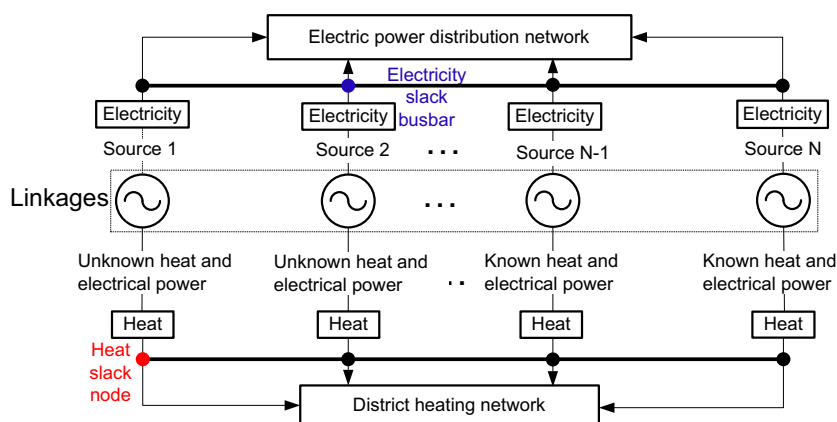

Fig. 1. Schematic diagram of the combined electricity and district heating networks in islanded mode.
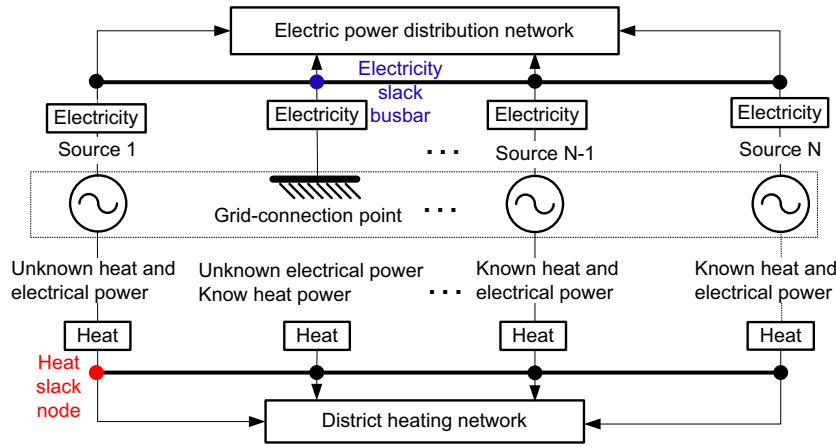
Fig. 2. Schematic diagram of the combined electricity and district heating networks in grid-connected mode.

Table 1
Known and unknown variables of electricity and heat networks.

	Variables	Known	Unknown
Electricity networks	Voltage angle θ	At the slack busbar	At all busbars except the slack busbar
	Active power P	At all busbars except the slack busbar	At the slack busbar
	Voltage magnitude $|V|$	At each PV busbar	At each PQ busbar
	Reactive power Q	At each PQ busbar	At each PV busbar
Heat networks	Pressure head H	At one given node	At all nodes except the given node
	Heat power Φ	At all nodes except the slack node	At the slack node
	Supply temperature T_s	At each source node	At each load node
	Return temperature T_r	At each load node (before mixing)	At each source node
	Mass flow rate		Within each pipe

Table 2
Analogues of busbar and node types in electrical and thermal power flows.

Electrical power flow	PQ busbar	PV busbar	$V\theta$ busbar
Thermal power flow	ΦT_r node	ΦT_s node	$T_s H$ node

the electrical power generated from this unit. Similarly, the electrical power generated from Source 1 (at the heat slack node) is a function of the heat network. Neither the heat network nor the electricity network can be analysed without taking into account the other network.

The power flow formulation of a district heating network is similar to that of an electrical network. The AC electrical power flow model for electrical networks is well established [27,28]. An integrated hydraulic-thermal calculation technique of district heating networks, the so-called thermal power flow was described in this paper. Based on these two power flows, an integrated electrical-hydraulic-thermal calculation technique, the so-called integrated power flow was developed using the Newton–Raphson method. In the integrated power flow, the known and unknown variables of electricity and heat networks are shown in Table 1.

The analogues of three types of busbars and nodes in the electrical and thermal power flows are shown in Table 2. Each type of busbar and node is classified according to two known quantities.

3. Analysis of district heating networks

District heating networks usually consist of supply and return pipes that deliver heat, in the form of hot water or steam, from the point of generation to the end consumers [12,29]. In a

simulation of a district heating network, the variables are: pressure and mass flow rates in the hydraulic model; supply and return temperatures and heat power in the thermal model. Hydraulic and thermal analysis is carried out to determine the mass flow rates within each pipe and the supply and return temperatures at each node. Usually, hydraulic analysis is carried out before the thermal analysis [29–32]. It is common to perform hydraulic calculations using the Hardy-Cross or Newton–Raphson methods [29–33]. The Hardy-Cross method considers each loop independently and the Newton–Raphson method considers all loops simultaneously [29]. The decomposed hydraulic and thermal analysis of a pipe network using the Newton–Raphson method is described in [30].

An integrated hydraulic-thermal model of district heating networks, solved by the Newton–Raphson method, was used in this study. In the hydraulic model, the network description is based on a graph-theoretical method. In the thermal model, a matrix approach was used.

3.1. Hydraulic model

3.1.1. Continuity of flow

The continuity of flow is expressed as: the mass flow that enters into a node is equal to the mass flow that leaves the node plus the flow consumption at the node. For the entire hydraulic network, the continuity of flow is expressed as

$$\boldsymbol{A\dot{m}} = \boldsymbol{\dot{m}_q} \tag{1}$$

where $\boldsymbol{A}$ is the network incidence matrix that relates the nodes to the branches; $\boldsymbol{\dot{m}}$ is the vector of the mass flow (kg/s) within each pipe; $\boldsymbol{\dot{m}_q}$ is the vector of the mass flow (kg/s) through each node injected from a source or discharged to a load.

3.1.2. Loop pressure equation

Head loss is the pressure change in *metres* due to the pipe friction [32]. The loop pressure equation states that the sum of head losses around a closed loop must be equal to zero. For the entire hydraulic network, the loop pressure equation is expressed as

$$\boldsymbol{B}\, \boldsymbol{h}_f = 0 \tag{2}$$

where $\boldsymbol{B}$ is the loop incidence matrix that relates the loops to the branches; and $\boldsymbol{h}_f$ is the vector of the head losses (m).

3.1.3. Head loss equation

The relation between the flow and the head losses along each pipe is

$$\boldsymbol{h}_f = \boldsymbol{K}\, \dot{m}|\dot{m}| \tag{3}$$

where $\boldsymbol{K}$ is the vector of the resistance coefficients of each pipe. $\boldsymbol{K}$ generally depends largely on the diameter of a pipe. The resistance coefficient $\boldsymbol{K}$ of a pipe is calculated from the friction factor $\boldsymbol{f}$. The details are described in reference [34].

Hence, Eq. (2) is expressed as

$$\boldsymbol{B}\, \boldsymbol{K}\, \dot{m}|\dot{m}| = \sum_{j=1}^{n_{pipe}} B_{ij} k_j \dot{m}_j |\dot{m}_j| = 0 \tag{4}$$

where n_{pipe} is the number of pipes; i is the index of loops and j is the index of pipes.

3.2. Thermal model

The thermal model is used to determine the temperatures at each node. There are three different temperatures associated with each node (Fig. 3): the supply temperature (T_s); the outlet temperature (T_o) and the return temperature (T_r) [35]. The outlet temperature is defined as the temperature of the flow at the outlet of each node before mixing in the return network. If there is no flow mixing at a node, then the outlet temperature T_o is equal to the return temperature T_r at this node. Usually, the supply temperatures T_s at each source and the outlet temperatures T_o at each load are specified in the thermal model [29,31,36,37]. The load outlet temperature T_o depends on the supply temperature T_s, the outdoor temperature and the heat load [38–41]. For simplicity, the outlet temperature T_o is assumed to be known at each load.

The heat power is calculated using equation [29,41]

$$\boldsymbol{\Phi} = C_p \dot{m}_q (\boldsymbol{T}_s - \boldsymbol{T}_0) \tag{5}$$

where $\boldsymbol{\Phi}$ is the vector of heat power (W_{th}) consumed or supplied at each node; the subscript *th* represents *thermal*; C_p is the specific heat of water (J kg^{-1} °C^{-1}), $C_p = 4.182 \times 10^{-3}$ MJ kg^{-1} °C^{-1}); and $\dot{m}_q$ is the vector of the mass flow rate (kg/s) through each node injected from a supply or discharged to a load.

The temperature at the outlet of a pipe is calculated using equation [29,41,42].

$$T_{end} = (T_{start} - T_a)e^{-\frac{\lambda L}{C_p \dot{m}}} + T_a \tag{6}$$

where T_{start} and T_{end} are the temperatures at the start node and the end node of a pipe (°C); T_a is the ambient temperature (°C); λ is the overall heat transfer coefficient of each pipe per unit length (W m^{-1} °C^{-1})); L is the length of each pipe (m); and $\dot{m}$ is the mass flow rate (kg/s) within each pipe.

Eq. (6) shows that if the mass flow rate within a pipe is larger, the temperature at the end node of the pipe is larger and the temperature drop along the pipe is smaller.

For brevity, denoting $T'_{start} = T_{start} - T_a$, $T'_{end} = T_{end} - T_a$, $\Psi = e^{-\frac{\lambda L}{C_p \dot{m}}}$, thus Eq. (6) is written as
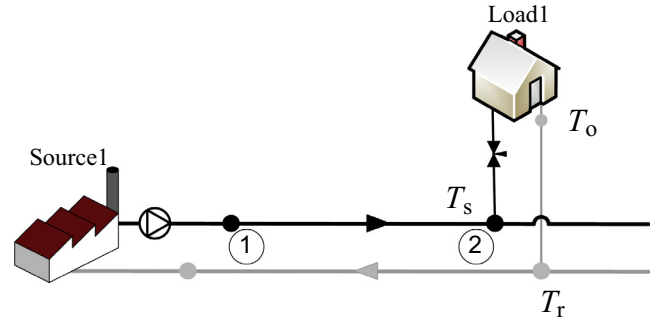
$$T'_{end} = T'_{start}\Psi \tag{7}$$

Fig. 3. Temperatures associated with each node.

The temperature of water leaving a node with more than one incoming pipe is calculated as the mixture temperature of the incoming flows using Eq. (8). Temperature at the start of each pipe leaving the node is equal to the mixture temperature at the node [29,41,43]

$$\left(\sum \dot{m}_{out}\right)T_{out} = \sum(\dot{m}_{in}T_{in}) \tag{8}$$

where T_{out} is the mixture temperature of a node (°C); $\dot{m}_{out}$ is the mass flow rate within a pipe leaving the node (kg/s); T_{in} is the temperature of flow at the end of an incoming pipe (°C); and $\dot{m}_{in}$ is the mass flow rate within a pipe coming into the node (kg/s).

For a district heating network, the thermal model determines the supply temperatures at each load and the return temperatures at each load and source. The assumptions are that supply temperatures at each source and return temperatures at each load before mixing are specified, as well as mass flow rates within each pipe [29,31,36,37]. The problem becomes complex when the thermal model equations are applied to a district heating network with arbitrary topology. Therefore, a matrix formulation of a thermal model was used. Furthermore, a general program for the thermal model in a district heating network was developed in MATLAB.

3.3. Hydraulic-thermal model

For a district heating network, the objective of the hydraulic-thermal model is to determine the mass flow rates $\dot{m}$ within each pipe, the load supply temperatures and the source return temperatures. It is assumed that the source supply temperatures and the load return temperatures are specified; the mass flow rates $\dot{m}_q$ or the heat power $\boldsymbol{\Phi}$ are specified at all nodes except the slack node [29,31,36,37]. The slack node is defined to supply the heat power difference between the total system loads plus losses and the sum of specified heat power at the source nodes.

If the nodal injected mass flow rate $\dot{m}_q$ is specified, the hydraulic-thermal model calculations are performed independently [30,43]. Firstly, the pipe mass flow rate $\dot{m}$ is calculated by the hydraulic model. Then, the results of the hydraulic model $\dot{m}$ are substituted into the thermal model. Finally, the load supply temperatures and the source return temperatures are calculated by the thermal model.

Alternatively, if the heat power $\boldsymbol{\Phi}$ consumed or supplied at each node is specified, two methods are adopted to perform the calculation of the hydraulic-thermal model. Conventionally, the calculation is through an iterative procedure – referred to as the decomposed hydraulic-thermal method – between the individual hydraulic and thermal models [31]. In this paper, an integrated hydraulic-thermal method was proposed, in which the hydraulic and thermal models were combined in a single system of equations. The two methods were described together with the integration of the electrical power flow model in Section 5.

The integrated calculation combines the individual hydraulic and thermal analyses using the Newton–Raphson approach. It takes into account the coupling between the individual hydraulic and thermal analyses. For instance, the thermal calculation cannot be performed without knowing the pipe mass flows. The hydraulic calculation cannot be performed without knowing temperatures under the assumption that the nodal heat power is specified.

The proposed methods can handle the initial conditions with arbitrary flow directions. During each iteration, the network incidence matrix A and the loop incidence matrix B are updated according to the signs of the pipe mass flow rates. Based on matrix A, the formulation of the temperature mixing equations in the thermal model is updated at each iteration.

4. Electrical power flow analysis

Given a power system described by an admittance matrix, and given a subset of voltage magnitudes, voltage angles and real and reactive power injections, the electrical power flow determines the other voltage magnitudes and angles, and real and reactive power injections.

The voltage V at busbar i is given by

$$V_i = |V_i| \angle \theta_i = |V_i| e^{j\theta_i} = |V_i|(\cos\theta_i + j\sin\theta_i) \tag{9}$$

where $|V|$ is the voltage magnitude (p.u.). θ is the voltage angle (rad). j is the imaginary unit.

The current injected into the network at busbar i is given by

$$I_i = \sum_{n=1}^{N} Y_{in} V_n \tag{10}$$

where N is the number of busbars in the electricity network; Y is the admittance matrix that relates current injection at a busbar to the busbar voltage. Current injections may be either positive (into the busbar) or negative (out of the busbar).

Thus, the calculated complex power injected at busbar i is

$$S_i = P_i + jQ_i = V_i I_i^* = V_i \sum_{n=1}^{N} (Y_{in} V_n)^* \tag{11}$$

Eq. (11) constitutes the polar form of the electrical power flow equations.

The specified complex power being injected into the network at busbar i is the complex power difference between the source and the load.

$$S_i^{sp} = S_{i,source} - S_{i,load} \tag{12}$$

Following Eqs. (11) and (12), the electrical complex power mismatches ΔS_i injected at busbar i are denoted as the specified value S_i^{sp} minus the calculated value S_i.

$$\Delta S_i = S_i^{sp} - S_i = S_i^{sp} - V_i \sum_{n=1}^{N} (Y_{in} V_n)^* \tag{13}$$

Following Eq. (13), the diagonal and off-diagonal elements are calculated as [44]

$$J_{S_\theta} = \frac{\partial \Delta S_i}{\partial \theta_k} = \begin{cases} j V_i Y_{ik}^* V_k^* & k \neq i \\ j V_i Y_{ii}^* V_i^* - jS_i & k = i \end{cases} \tag{14}$$

$$J_{S_V} = \frac{\partial \Delta S_i}{\partial |V_k|} = \begin{cases} -V_i Y_{ik}^* e^{-j\theta_k} & k \neq i \\ -V_i Y_{ii}^* e^{-j\theta_i} - S_i/|V_i| & k = i \end{cases} \tag{15}$$

Thus, the electricity Jacobian matrix is constituted as

$$J_e = \begin{bmatrix} Real(J_{S_\theta}) & Real(J_{S_V}) \\ Imag(J_{S_\theta}) & Imag(J_{S_V}) \end{bmatrix} \tag{16}$$

where *Real* represents the real part of a complex expression and *Imag* represents the imaginary part of a complex expression.

Hence, the iterative form of the Newton–Raphson method is

$$\begin{bmatrix} \theta \\ |V| \end{bmatrix}^{(i+1)} = \begin{bmatrix} \theta \\ |V| \end{bmatrix}^{(i)} - J_e^{-1} \begin{bmatrix} \Delta P \\ \Delta Q \end{bmatrix} \tag{17}$$

where θ is the vector of voltage angles at non-slack busbars; $|V|$ is the vector of voltage magnitudes at PQ busbars; ΔP is the vector of active power at non-slack busbars; and ΔQ is the vector of reactive power at PQ busbars.

5. Combined analysis

Two methods for combined analysis were developed to investigate the performance of electricity and heat networks. The methods are based on the hydraulic-thermal model of heat networks and the electrical power flow model.

For the power flow analysis, the electrical power at each busbar is specified except for the slack busbar. Heat power is specified at each node except for the slack node. Thus, the linkages between electrical and heat networks are the generation components (CHP units or electric boilers) at the slack busbar or slack node, and the non-generation components such as the circulation pumps.

The assumptions for the example network shown in Fig. 1 are as follows:

(1) Source 1 is connected to the heat slack node and Source 2 connected to the electricity slack busbar.
   a. In *grid-connected mode*, Source 1 corresponds to a gas turbine CHP unit and Source 2 corresponds to the connection to the grid.
   b. In *islanded mode*, Source 1 corresponds to a steam turbine CHP unit and Source 2 corresponds to a gas turbine CHP unit.
(2) The heat-to-power ratio of the gas turbine CHP unit is constant and the gas turbine CHP unit can be operated at partial load conditions to respond to electricity and heat load variation.
(3) The fuel input rate to the steam turbine CHP unit is constant and the heat-to-power ratio of the steam turbine CHP unit can be modulated.
(4) The heat power generated by CHP units is fully utilised, without the waste of heat.

Two calculation techniques were developed to calculate the operating points of the electricity and heat networks.

1. In the *decomposed* electrical-hydraulic-thermal method, the independent hydraulic equations and thermal equations, and electrical power flow equations were calculated sequentially and linked through the coupling components. The sequential procedure is iterated at each time step until the solution converges to an acceptable tolerance.
2. In the *integrated* electrical-hydraulic-thermal method, the electrical power flow equations, the hydraulic equations, and the thermal equations were combined and solved simultaneously as an integrated whole.

The structure of the integrated electrical-hydraulic-thermal method is shown in Fig. 4. The hydraulic and thermal model equations are linked through the mass flow rates. The electrical power flow equations and hydraulic-thermal model equations are linked through the coupling components.

5.1. Decomposed electrical-hydraulic-thermal method

In *grid-connected mode*, the hydraulic-thermal model is solved first. Then these results are transferred to the electricity network through the coupling components (CHP units, heat pumps, electric boilers and circulation pumps). Finally the electrical power flow model is solved. In *grid-connected mode*, any surplus or deficit in electrical power is supplied from the main grid and there is no heat generated at the electricity slack busbar. Therefore, the independent hydraulic model, thermal model and electrical power flow model are solved sequentially only once without iteration.

In *islanded mode*, the independent hydraulic and thermal model and electrical power flow model are solved sequentially. This sequential procedure is iterated until the solution converges to an acceptable tolerance.

The flowchart of the decomposed electrical-hydraulic-thermal method is shown in Fig. 5. Both grid-connected mode and islanded mode are considered, and the islanded mode is highlighted in blue.

In the flowchart shown in Fig. 5, the input data and the initialised variables are shown in Table 1. Based on these variables, the nodal mass flow rates $\dot{\boldsymbol{m}}_q$ are calculated using the heat power Eq. (5).

The heat power from Source 1 at the heat slack node is denoted as $\emptyset_{1,source}$. The electrical power from Source 1 is denoted as $P_{1,source}$. The heat power from Source 2 at the electricity slack busbar is denoted as $\emptyset_{2,source}$. The electrical power from Source 2 is denoted as $P_{2,source}$. Here, the electrical power represents active power. Heat power from a Source is related with its generated active power and vice versa.

$\Phi_{1,source}$ is calculated from the results of the decomposed hydraulic-thermal method using the heat power Eq. (5).

$$\emptyset_{1,source} = C_p \boldsymbol{A}_{1,source} \dot{\boldsymbol{m}}(T_{s1,source} - T_{r1,source}) \tag{18}$$

where $\boldsymbol{A}_{1,source}$ is a row of the network incidence matrix $\boldsymbol{A}$ that relates Source 1 at the heat slack node; $T_{s1,source}$ and $T_{r1,source}$ are the supply temperature and return temperature at Source 1.

$P_{1,source}$ is determined by $\Phi_{1,source}$.

$$P_{1,CHP} = \begin{cases} \emptyset_{1,source}/c_{m1}, & \text{gas turbine} \\ -\emptyset_{1,source}/Z + \eta_e F_{in}, & \text{steam turbine} \end{cases} \tag{19}$$

where c_{m1} is the heat-to-power ratio of the gas turbine CHP1; Z is the ratio that describes the trade-off between heat supplied to the site and the electrical power of the extraction steam turbine CHP1 [45]; η_e is the electrical efficiency of the unit in full condensing mode; F_{in} (MW) is the fuel input rate of the steam turbine unit, which is held constant in this paper.

The total electrical power supplied from Source 1 is decreased by the pump electrical power consumption and thus Eq. (19) is

$$P_{1,source} = P_{1,CHP} - P_p \tag{20}$$

where P_p is the electrical power consumed (MW$_e$) by the pump; the subscript e represents electrical.

$P_{2,source}$ is calculated from the results of the electrical power flow calculation using Eq. (11), plus the pump electrical power consumption.

$$P_{2,source} = Real\left\{ V_{2,source} \sum_{k=1}^{N} (Y_{ik}V_k)^* \right\} + P_p \tag{21}$$

In islanded mode, $\Phi_{2,source}$ is determined by $P_{2,source}$.

$$\emptyset_{2,source} = c_{m2} P_{2,source} \tag{22}$$

where c_{m2} is the heat-to-power ratio of the CHP unit at Source 2.

In Fig. 6 the procedure of determining the heat and electrical power generated from Source 1 and Source 2 is illustrated. The left line that slopes downward describes the performance curve of an extraction steam turbine CHP unit at Source 1 and the slope is equal to the negative of the Z ratio of Source 1 ($-Z$). The right line that slopes upward describes the performance curve of a gas turbine CHP unit at Source 2 and the slope is equal to the heat-to-power ratio of Source 2 (c_{m2}).

Following the flowchart as shown in Fig. 5, the steps used to solve the model as illustrated in Fig. 6 are as follows:

(1) Start with the known variables as shown in Table 1 and network parameters.
(2) Assume the initial conditions for the heat and electricity networks. Iteration $i = 1$.
(3–6) Solve the hydraulic and thermal model, represented as the red dashed arrow $a \rightarrow b$ when $i = 1$.
(7) Calculate $\emptyset_{1,source}^{(i)}$, represented as a horizontal dotted line.
(8) Calculate $P_{1,source}^{(i)}$, represented as a vertical dotted line, according to the performance curve of Source 1 using Eq. (19).
(9) Solve the electrical power flow model, represented as the blue solid arrow $b \rightarrow c$ when $i = 1$.
(10) Calculate $P_{2,source}^{(i)}$, represented as a vertical solid line.
(11) Calculate $\emptyset_{2,source}^{(i)}$, represented as a horizontal solid line, according to the performance curve of Source 2 using Eq. (22).
(12) This procedure is repeated from step 3 until $\Delta\emptyset_{2,source}^{(i)} = \emptyset_{2,source}^{(i)} - \emptyset_{2,source}^{(i-1)}$ becomes less than the tolerance $\varepsilon = 10^{-3} \cdot i = i + 1$.

5.2. Integrated electrical-hydraulic-thermal method

In the integrated electrical-hydraulic-thermal method, the electrical power flow equations, the hydraulic equations and the thermal equations were combined to form a single system of equations and solved simultaneously as an integrated whole using the Newton–Raphson method. The structure of the calculation technique is shown in Fig. 4 and the flowchart is shown in Fig. 7. Both grid-connected mode and islanded mode are considered, and the islanded mode is highlighted in[1] blue.

In *grid-connected mode*, any surplus or deficit in electrical power is supplied from the main grid and there is no heat generated at the electricity slack busbar. Thus, the derivative of the heat power mismatches with respect to the electrical variables is zero, which means the lower off-diagonal submatrix of the integrated Jacobian matrix is zero.

While in *islanded mode*, the heat generated at the electricity slack busbar ($\Phi_{2,source}$) is a function of the electricity network, which means the lower off-diagonal submatrix of the integrated Jacobian matrix is nonzero.

The iterative form of the Newton–Raphson method is

$$\boldsymbol{x}^{(i+1)} = \boldsymbol{x}^{(i)} - \boldsymbol{J}^{-1}\Delta\boldsymbol{F} \tag{23}$$

where i is the iteration number; $\boldsymbol{x}$ is the vector of state variables as shown in Eq. (24); $\Delta\boldsymbol{F}$ is the vector of total mismatches as shown in Eq. (25); and $\boldsymbol{J}$ is the Jacobian matrix as shown in Eq. (26).

$$\boldsymbol{x} = \begin{bmatrix} \boldsymbol{\theta} \\ |\boldsymbol{V}| \\ \dot{\boldsymbol{m}} \\ \boldsymbol{T}'_{s,load} \\ \boldsymbol{T}'_{r,load} \end{bmatrix} \tag{24}$$

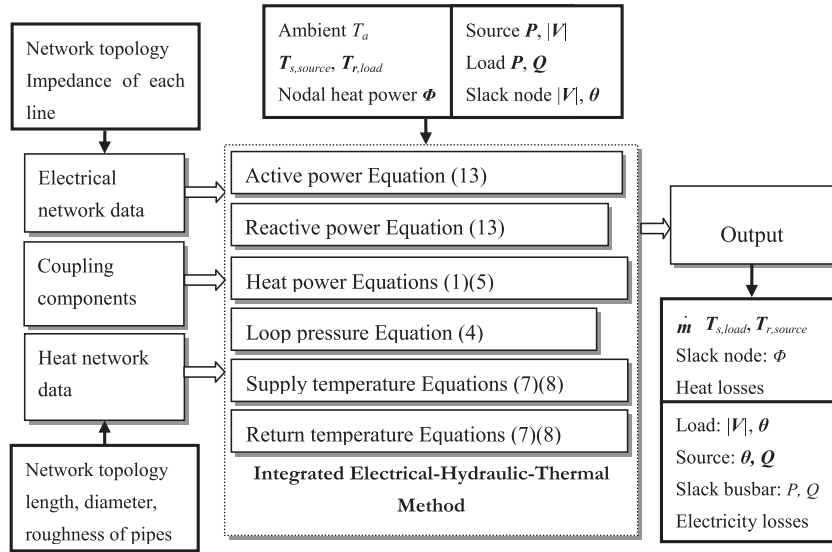[1] For interpretation of colour in Fig. 7, the reader is referred to the web version of this article.

Fig. 4. Structure of the integrated electrical-hydraulic-thermal method.

Fig. 5. Flowchart of the decomposed electrical-hydraulic-thermal method.

Following the structure of the integrated electrical-hydraulic-thermal method as shown in Fig. 4, $\Delta \boldsymbol{F}$ is expressed as

$$
\Delta \boldsymbol{F} = \begin{bmatrix} \Delta \boldsymbol{P} \\ \Delta \boldsymbol{Q} \\ \Delta \boldsymbol{\Phi} \\ \Delta \boldsymbol{p} \\ \Delta \boldsymbol{T}'_s \\ \Delta \boldsymbol{T}'_r \end{bmatrix} = \begin{bmatrix} \boldsymbol{P}^{sp} - Real\{\boldsymbol{V}(\boldsymbol{YV})^*\} \\ \boldsymbol{Q}^{sp} - Imag\{\boldsymbol{V}(\boldsymbol{YV})^*\} \\ C_p \boldsymbol{A}\dot{\boldsymbol{m}}(\boldsymbol{T}_s - \boldsymbol{T}_o) - \boldsymbol{\Phi}^{sp} \\ \boldsymbol{B}\,k\dot{\boldsymbol{m}}|\dot{\boldsymbol{m}}| - \boldsymbol{0} \\ \boldsymbol{C}_s \boldsymbol{T}'_{s,load} - \boldsymbol{b}_s \\ \boldsymbol{C}_r \boldsymbol{T}'_{r,load} - \boldsymbol{b}_r \end{bmatrix} \begin{array}{l} \leftarrow Active\ power\ mismatches \\ \leftarrow Reactive\ power\ mismatches \\ \leftarrow Heat\ power\ mismatches \\ \leftarrow Loop\ pressure\ mismatches \\ \leftarrow Supply\ temperature\ mismatches \\ \leftarrow Return\ temperature\ mismatches \end{array}
$$

(25)

where $\boldsymbol{C}_s$ is a matrix of coefficients for supply temperature calculation and $\boldsymbol{C}_r$ is a matrix of coefficients for return temperature calculation. Their calculations in detail were described in [34]. The superscript *sp* represents *specified*.

Conventionally, for electrical power flow analysis, the vector $\boldsymbol{P}^{sp}$ in the active power mismatches is specified. While for the integrated electrical-hydraulic-thermal method, in the mismatches $\Delta \boldsymbol{F}$ in Eq. (25), the element $P_{1,source}$ of the vector $\boldsymbol{P}^{sp}$ is determined from the heat power generated at the heat slack node and it is expressed as a function of the heat network. Thus, the derivative of the electrical power mismatches ($\Delta \boldsymbol{P}$) with respect to the heat variables ($\dot{\boldsymbol{m}}$) is nonzero $\left(\frac{\partial P_{1,source}}{\partial \dot{\boldsymbol{m}}}\right)$.

Conventionally, for hydraulic and thermal analysis, the vector $\boldsymbol{\Phi}^{sp}$ in the heat power mismatches is specified. While for the integrated method in *islanded mode*, the element $\emptyset_{2,source}$ of the vector $\boldsymbol{\Phi}^{sp}$ is expressed as a function of the electricity network. Thus, the derivative of the heat power mismatches ($\Delta \boldsymbol{\Phi}$) with respect to the electrical variables ($\theta, |\boldsymbol{V}|$) is nonzero.

The integrated Jacobian matrix $\boldsymbol{J}$ is derived from the mismatches $\Delta \boldsymbol{F}$. It consists of four submatrices: electricity submatrix $\boldsymbol{J}_e$, electricity to heat submatrix $\boldsymbol{J}_{eh}$, heat to electricity submatrix $\boldsymbol{J}_{he}$ and heat submatrix $\boldsymbol{J}_h$.

$$
\boldsymbol{J} = \begin{bmatrix} \boldsymbol{J}_e & \boldsymbol{J}_{eh} \\ \boldsymbol{J}_{he} & \boldsymbol{J}_h \end{bmatrix} = \begin{bmatrix} \frac{\partial \Delta P}{\partial \theta} & \frac{\partial \Delta P}{\partial |V|} & \frac{\partial \Delta P}{\partial \dot{m}} & \frac{\partial \Delta P}{\partial T} \\ \frac{\partial \Delta Q}{\partial \theta} & \frac{\partial \Delta Q}{\partial |V|} & \frac{\partial \Delta Q}{\partial \dot{m}} & \frac{\partial \Delta Q}{\partial T} \\ \frac{\partial \Delta \emptyset}{\partial \theta} & \frac{\partial \Delta \emptyset}{\partial |V|} & \frac{\partial \Delta \emptyset}{\partial \dot{m}} & \frac{\partial \Delta \emptyset}{\partial T} \\ \frac{\partial \Delta T}{\partial \theta} & \frac{\partial \Delta T}{\partial |V|} & \frac{\partial \Delta T}{\partial \dot{m}} & \frac{\partial \Delta T}{\partial T} \end{bmatrix}
$$

(26)

where the shaded block matrices are nonzero and the others are zero. The off-diagonal submatrix highlighted in blue is zero in grid-connected mode and nonzero in islanded mode.
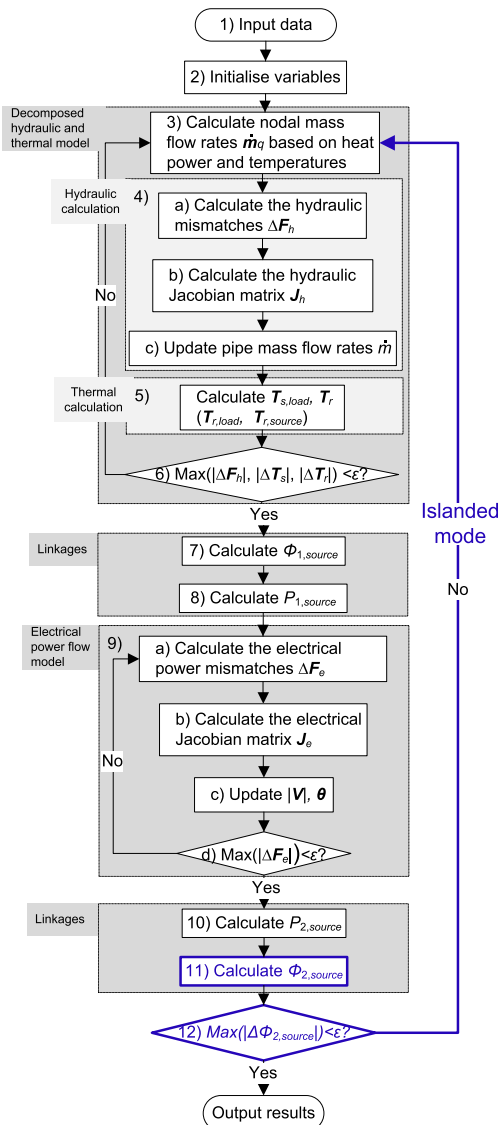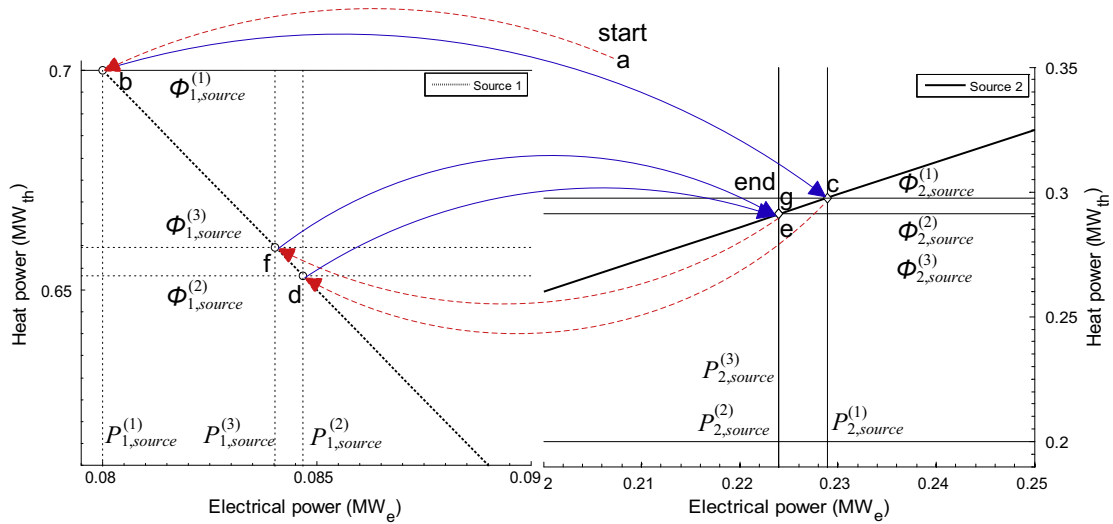
Fig. 6. Procedure to calculate the electrical and heat power from both Source 1 and Source 2 that link electricity and heat networks.
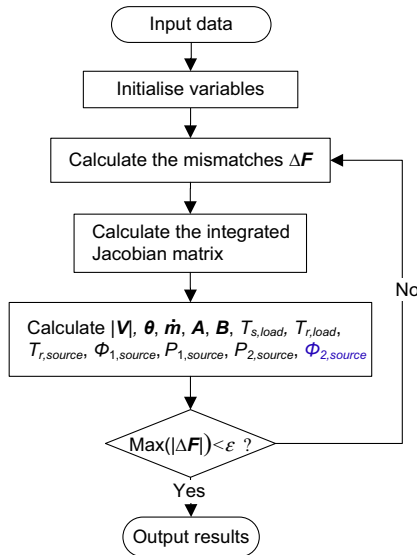

Fig. 7. Flowchart of the integrated electrical-hydraulic-thermal method.

For $\boldsymbol{J}_{eh}$, the vector of the nonzero elements $\frac{\partial P_{1,source}}{\partial \dot{\boldsymbol{m}}}$ is calculated using Eqs. (18) and (19)

$$\frac{\partial P_{1,source}}{\partial \dot{\boldsymbol{m}}} = \frac{\partial P_{1,CHP}}{\partial \dot{\boldsymbol{m}}} \begin{cases} C_p \boldsymbol{A}_{1,source}(T_{s1,source} - T_{r1,source})/c_{m1}, gas\ turbine \\ -C_p \boldsymbol{A}_{1,source}(T_{s1,source} - T_{r1,source})/Z, steam\ turbine \end{cases} \tag{27}$$

where $\boldsymbol{A}_{1,source}$ is a row of the network incidence matrix $\boldsymbol{A}$ that relates to Source 1 at the heat slack node. In the return network, the term $T_{r1,source}$ is expressed as a function of the pipe mass flow rates $\dot{\boldsymbol{m}}$ and the load return temperatures $\boldsymbol{T}'_{r,load}$. For simplicity, the derivatives of the term $T_{r1,source}$ with respect to $\dot{\boldsymbol{m}}$ and $\boldsymbol{T}'_{r,load}$ are very small and are neglected.

In the case of circulation pumps, the derivative of the term P_p (the electrical power consumed by the pumps) with respect to $\dot{\boldsymbol{m}}$ in Eqs. (19) and (20) is very small and is neglected.

For $\boldsymbol{J}_{he}$, in grid-connected mode, the heat power is not a function of the electricity network thus $\boldsymbol{J}_{he} = \boldsymbol{0}$. In islanded mode, $\boldsymbol{J}_{he}$ is nonzero and the vector of the nonzero elements is calculated using Eqs. (21) and (22)

$$\left[\frac{\partial \emptyset_{2,source}}{\partial \theta_k} \quad \frac{\partial \emptyset_{2,source}}{\partial |V_k|} \right] = c_{m2} \left[Re\left(jV_i Y_{ik}^* V_k^*\right) \quad Re\left(-V_i Y_{ik}^* e^{-j\theta_k}\right) \right] \tag{28}$$

where the subscript i represents Source 2 at the electricity slack busbar.

The procedure used to illustrate the example networks linked by a CHP unit only is shown in Fig. 8. During each iteration, the electrical and heat power generated from two sources are obtained simultaneously, which are represented as the points on the performance curves (the left line that slopes downward and the right line that slopes upward) of two CHP units. Due to the scale of the graph, starting from the 6th points on two lines, the two points on two lines are then simultaneously moved to the next two points with the same index at each iteration. The iteration procedure is repeated until the maximum absolute value of elements in the mismatches $|\Delta \boldsymbol{F}|$ becomes less than the tolerance $\varepsilon = 10^{-3}$.

5.3. Optimal dispatch

As an addition to the power flow, the use of optimal dispatch was added to the combined analysis and was solved by the Newton–Raphson method. The heat and electrical power generated from all sources were unknown. For simplicity, the optimal dispatch of electricity generation only was considered in this study.

The heat and electrical power generated from Source 1 and Source 2 and non-slack Source 3 were unknown and their heat-to-power ratios were known (Table 3). Comparing to the power flow, it can be seen that one more variable was added. Thus, one more equation was added to solve the problem. This additional equation was formed using the equal-incremental-fuel-cost criterion [27,28,46].

The equal-incremental-fuel-cost criterion states that for optimum economy the incremental fuel cost should be identical for all contributing turbine-generator sets [27,28]. In this paper, the equal-incremental-fuel-cost criterion is applied to the electrical power of Source 2 and Source 3 ($P_{2,source}$ and $P_{3,source}$). The electrical power of Source 1 ($P_{1,source}$) is calculated from the heat power of Source 1 ($\emptyset_{1,source}$). These are illustrated as shown in Fig. 9.

6. Case study

To demonstrate the capabilities of the combined analysis, a case study was conducted. The decomposed and integrated calculation
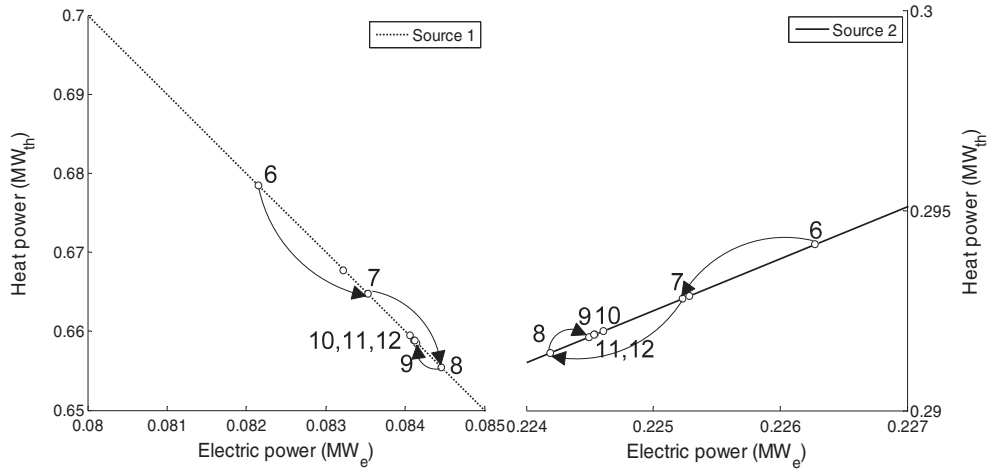
Fig. 8. Procedure to calculate the electrical and heat power from both Source 1 and Source 2 that link electricity and heat networks.

Table 3
Heat and electrical power from three sources.

	Source 1 (electricity slack busbar)	Source 2 (heat slack node)	Source 3 (non-slack)
Heat power	Unknown	Unknown	Unknown
Electrical power	Unknown	Unknown	Unknown
Heat-to-power ratio or Z ratio	Known	Known	Known

techniques were used to investigate the electricity and district heating networks, as shown in Fig. 10. The heat network is a low temperature district heating network fed by three CHP units.

6.1. Network description

6.1.1. Electricity network

The schematic diagram of the electric power distribution network is shown in Fig. 11. The electrical power is supplied to 5 lumped electrical loads through an 11/0.433 kV transformer at each feeder. Source 1 is connected to the 11 kV distribution network through a 33/11.5 kV transformer. Busbar ix is the slack busbar.

For the electricity network, the following assumptions were made:

(1) The base apparent power is 1 MVA and base voltage is 11 kV.
(2) The impedance of 185 mm^2 cable is 0.164+j0.080 Ω/km [47].
(3) 33/11.5 kV 15 MVA transformer has an impedance of 18% and X/R ratio of 15 [47].
(4) Active power of 5 lumped electrical loads at each load busbar:
   $P_i = 0.2$ MW$_e$,
   $P_{iii} = 0.5$ MW$_e$,
   $P_{iv} = 0.5$ MW$_e$,
   $P_v = 0.2$ MW$_e$,
   $P_{vi} = 0.2$ MW$_e$.
5) Power factor of each electrical load: p.f. = 1.
6) Voltage magnitude of each Source:
   $|V_{1,source}| = 1.02$ p.u.,
   $|V_{2,source}| = 1.05$ p.u.,
   $|V_{3,source}| = 1.05$ p.u.
7) Voltage angle of Source 1: $\theta_{1,source} = 0°$.

Fig. 9. Illustration of optimal dispatch for combined electrical and heat power.

6.1.2. Heat network

The schematic diagram of the heat network is shown in Fig. 10. The network parameters are presented in Appendix A. It was assumed that the heat power of the loads is known. The heat power of the loads (MW$_{th}$) are shown in Fig. 10. The total heat power of all loads is 2.164 MW$_{th}$. Node 1, node 11 and node 31 correspond to three sources. Node 1 is the heat slack node.

It was assumed that:

(1) Supply temperature at each source: $T_{s,source} = 70$ °C.
(2) Outlet temperature (return temperature before mixing) at each heat load: $T_{o,load} = 30$ °C.

6.1.3. CHP units

For the gas turbine CHP unit at Source 1, the relation between the heat and electrical power generation was calculated using the equation:

$$c_{m1}\bigg| = \frac{\emptyset_{CHP1}}{P_{CHP1}} \tag{29}$$

where c_{m1} is the heat-to-power ratio, $c_{m1} = 1.3$ [48,49]. Φ_{CHP1} (MW$_{th}$) is the useful heat output. P_{CHP1} (MW$_e$) is the electrical power output. Both variables are unknown in this case study.

For the extraction steam turbine CHP unit at Source 2, the Z ratio was used to calculate the heat output [45]:

$$Z_2\bigg| = \frac{\Delta\emptyset_2}{\Delta P_2} = \frac{\emptyset_{CHP2} - \emptyset_{con2}}{P_{con2} - P_{CHP2}} \tag{30}$$

where Z_2 is the Z ratio, $Z_2 = 8.1$ [45]. $\Delta\emptyset_2$ is the increased heat recovery and ΔP is reduced electrical power output. Φ_{CHP2} (MW$_{th}$) is the useful heat output. P_{CHP2} (MW$_e$) is the electrical power output. Both variables are unknown in this case study. P_{con2} is the electrical power generation of the extraction unit in full condensing mode. In this mode, the heat generation is zero, thus $\emptyset_{con2} = 0$. In this case study, $P_{con2} = 0.6$ MW$_{th}$.
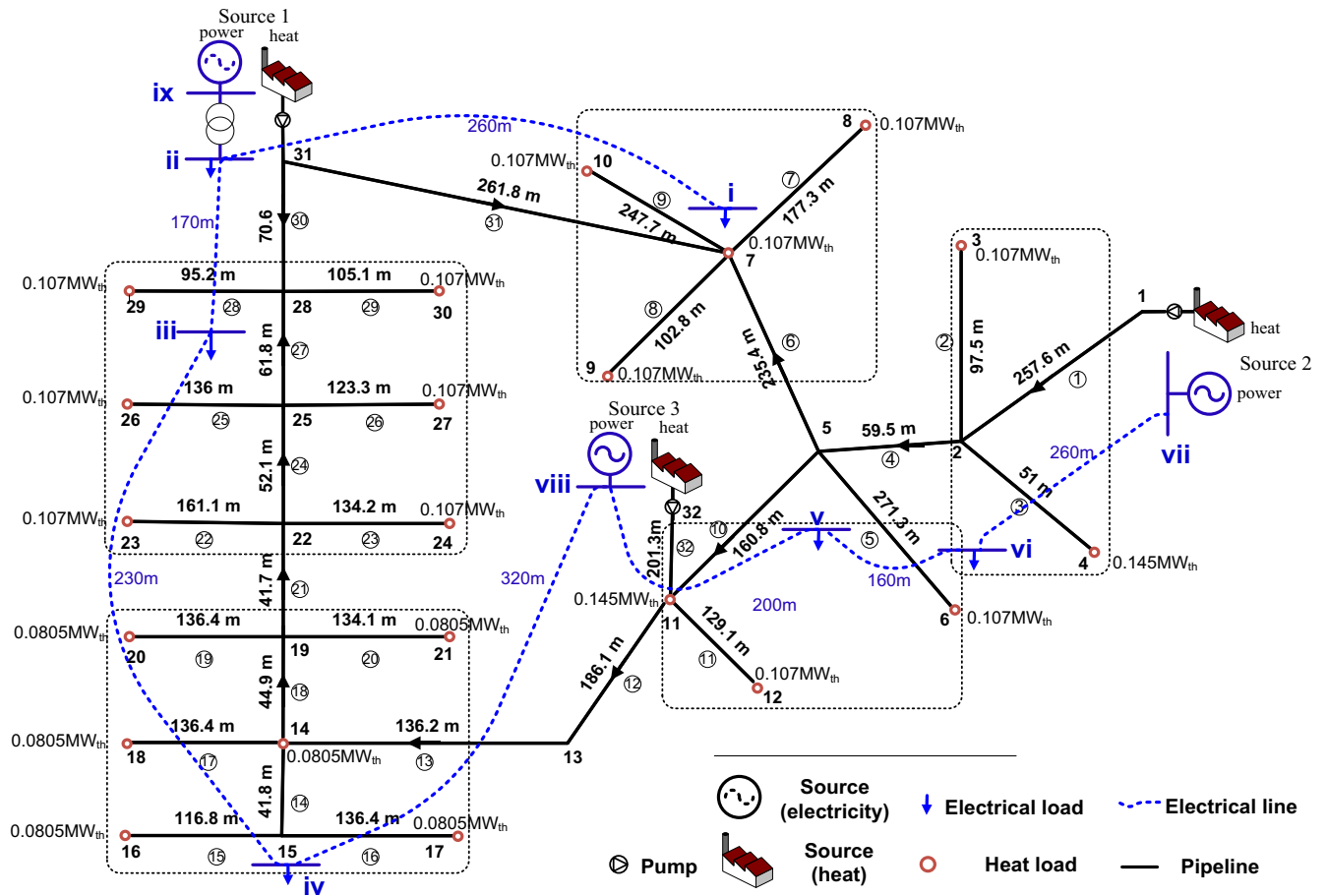
Fig. 10. Schematic diagram of the electricity and district heating networks of the Barry Island case study.
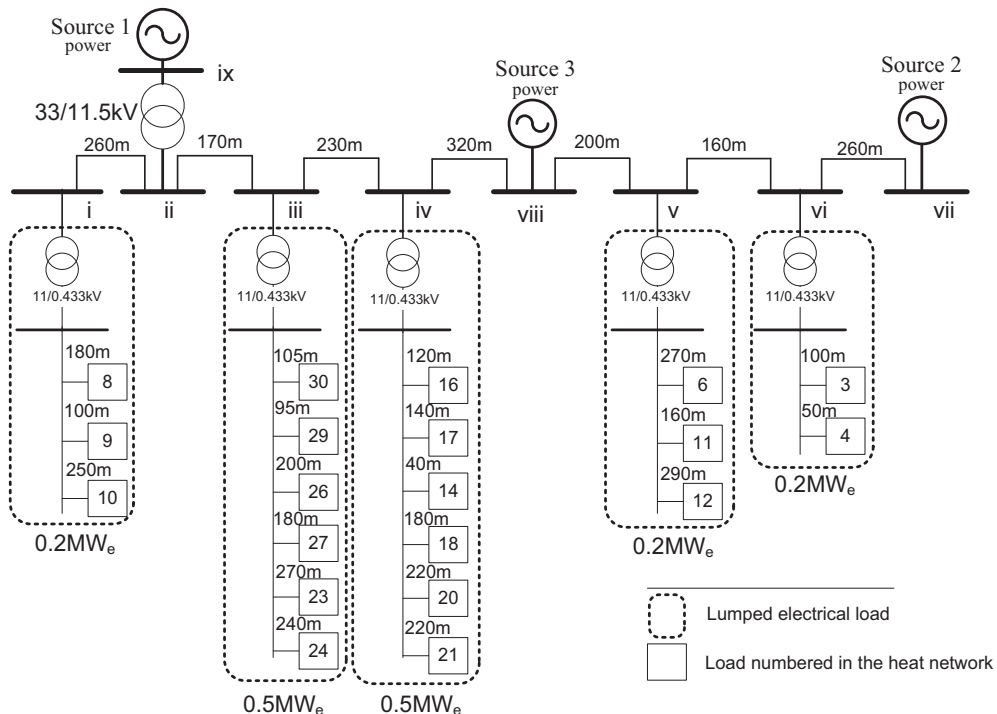

Fig. 11. Schematic diagram of the electric power distribution network of the Barry Island case study.

For the reciprocating engine CHP unit at Source 3, the relation between the heat and electrical power generation was calculated using the equation:

$$c_{m3} = \left| \frac{\emptyset_{CHP3}}{P_{CHP3}} \right. \tag{31}$$

where c_{m3} is the heat-to-power ratio, $c_{m3} = 1/0.79$ [49]. Φ_{CHP3} (MW_{th}) is the useful heat output. P_{CHP3} (MW_e) is the electrical power output. For the power flow, it is assumed that the electrical power generated from Source 3 is $P_{3,source} = 0.3\ MW_e$. Its calculated heat power is $\emptyset_{3,source} = c_{m3}\ P_{3,source} = 0.3797\ MW_{th}$. For the optimal dispatch, these are unknown.

It is assumed the fuel cost functions of Sources are:

$$f_{i,source} = a_i P_{i,source}^2 + b_i P_{i,source} + c_i \tag{32}$$

where $f_{i,source}$ is the fuel cost of Source i($£/h$). a_i, b_i and c_i are constants. $i = 1, 2, 3$. It is assumed $a_1 = 0.2$, $b_1 = 13$, $c_1 = 50$, $a_2 = 0.1$, $b_2 = 12.5$, $c_2 = 50$, $a_3 = 0.4$, $b_3 = 12$, $c_3 = 50$ [27].

6.2. Results

The Barry Island case study examined how electrical and heat demands in a self-sufficient system (no interconnection with external systems) were met using CHP units. The results of the decomposed and integrated methods were very close at 10^{-3} precision

and the results of the integrated method were presented. The variables of the electrical and heat networks with reference to peak heat load conditions were calculated as shown in Fig. 12.

For the power flow, the result of the heat and electrical power supplied from CHP units at Source 1, Source 2 and Source 3 was shown in Fig. 12 (a), where the generation of Source 3 was given.
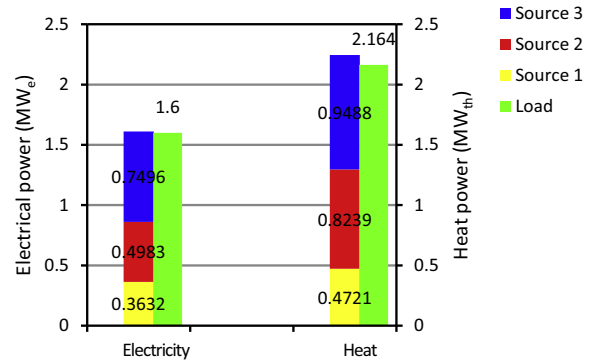
For the simple optimal dispatch, the results were shown in Fig. 12(b). The incremental fuel cost λ was calculated as 12.60 £/MW h. The total cost of Source 1, Source 2 and Source 3 for supplying electricity over an hour was: $54.75 + 56.25 + 59.22 = 170.22$ £/h. Substituting the power flow results as shown in Fig. 12(a) into the fuel cost function of the sources, the total fuel cost was calculated as 170.60 £/h. Comparing the two results, the solution of optimal dispatch saved 0.38 £/h.

For the power flow, the results of the calculation of the pipe mass flow rates were shown in Fig. 12(c). The main flow route 1–2–5–11–13–14–19–22–25–28–31–7–5 was indicated using bold lines. It is seen that in some pipes (○6, ○24 and ○27) the flows were of opposite direction compared with the initial guess, as shown in Fig. 10, and the mass flow rates were different. The mass flow rate within pipe ○12 was increased due to the flow injection from Source 3. The mass flow rate at node 31 was the largest since the heat power generated in Source 1 was the largest.
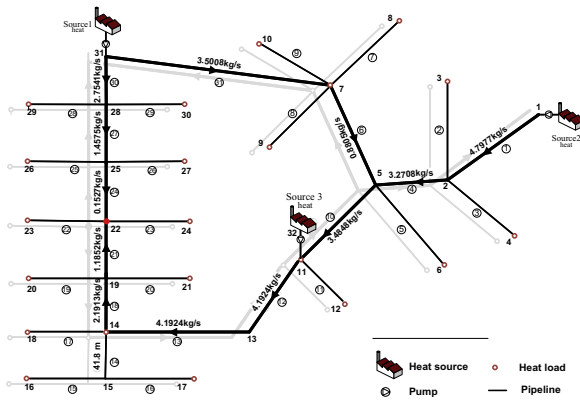
The results of the calculation of the supply and return temperatures at each node in the same main flow route were shown in Fig. 12(d). Node 22 is the end of two flow streams from Source
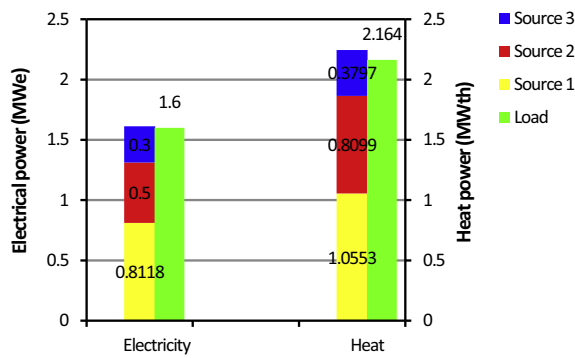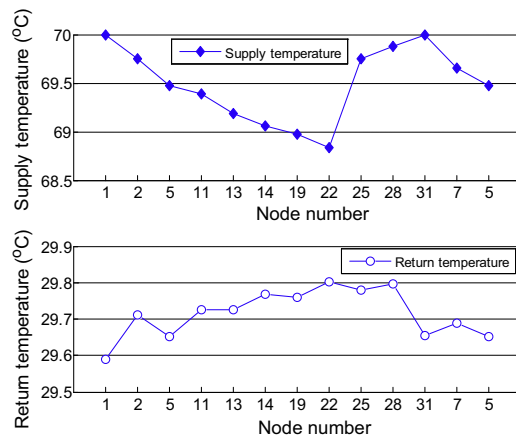

(a) Heat and electrical power supplied from three sources for the power flow analysis

(b) Heat and electrical power supplied from three sources for the simple optimal dispatch

(c) Pipe mass flow rates (kg/s) in a flow route

(d) Supply and return temperatures of the nodes in a flow route

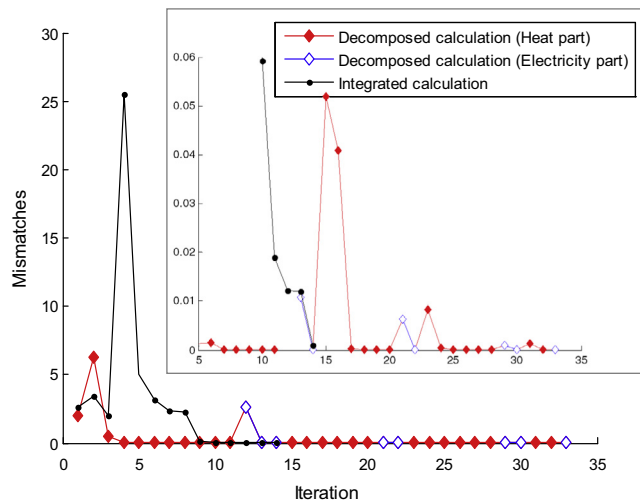**Fig. 12.** Results of the Barry Island case study.

Fig. 13. Convergence characteristics of the decomposed and integrated methods.

1 and Source 2 in the supply network and the start of the two flow streams in the return network. The lowest supply temperature and the highest return temperature were at node 22, where two opposite flow streams met.

In the main route of the supply network (Fig. 10), the flows mix at nodes 5 and 22 only. The supply temperature from node 1 to node 22 reduces gradually because of the heat losses.

In the same route of the return network, the flow mixing occurred at each node except node 13. Due to the mixing and due to the assumption that the return temperature from the consumer was fixed, the return temperature from node 22 to node 1 decreased unevenly.

Table 4
Pipe parameters for the Barry Island case study.

Pipe no.	From node	To node	Length (m)	Diameter (mm)	Heat transfer coefficient (W/mK)	Roughness (mm)
01	01	02	257.6	125	0.321	0.4
02	02	03	97.5	40	0.21	0.4
03	02	04	51	40	0.21	0.4
04	02	05	59.5	100	0.327	0.4
05	05	06	271.3	32	0.189	0.4
06	05	07	235.4	65	0.236	0.4
07	07	08	177.3	40	0.21	0.4
08	07	09	102.8	40	0.21	0.4
09	07	10	247.7	40	0.21	0.4
10	05	11	160.8	100	0.327	0.4
11	11	12	129.1	40	0.21	0.4
12	11	13	186.1	100	0.327	0.4
13	13	14	136.2	80	0.278	0.4
14	14	15	41.8	50	0.219	0.4
15	15	16	116.8	32	0.189	0.4
16	15	17	136.4	32	0.189	0.4
17	14	18	136.4	32	0.189	0.4
18	14	19	44.9	80	0.278	0.4
19	19	20	136.4	32	0.189	0.4
20	19	21	134.1	32	0.189	0.4
21	19	22	41.7	65	0.236	0.4
22	22	23	161.1	32	0.189	0.4
23	22	24	134.2	32	0.189	0.4
24	22	25	52.1	65	0.236	0.4
25	25	26	136	32	0.189	0.4
26	25	27	123.3	32	0.189	0.4
27	25	28	61.8	40	0.21	0.4
28	28	29	95.2	32	0.189	0.4
29	28	30	105.1	32	0.189	0.4
30	31	28	70.6	125	0.321	0.4
31	31	7	261.8	125	0.321	0.4
32	32	11	201.3	125	0.321	0.4

Voltage magnitudes at each load and voltage angles at each busbar in the electricity network were calculated.

To validate the results of the heat network analysis, the same heat network as shown in Fig. 10 was built using commercial software SINCAL [31]. The heat power of the CHP unit at Source 1 was specified in SINCAL based on the calculated value from the combined analysis ($\Phi_{CHP1} = 1.0553$ MW$_{th}$). The results of the heat network obtained using the combined analysis were the same as that obtained by SINCAL at 10^{-3} precision.

To validate the results of the electricity network analysis, the same electricity network as shown in Fig. 11, was built using commercial software IPSA [50]. The electrical power of the CHP unit at Source 2 was specified in IPSA based on the calculated value from the combined analysis ($P_{CHP2} = 0.5000$ MW$_e$). The results of the electricity network obtained using the combined analysis were the same as that obtained by IPSA.

Two methods were used in this study: decomposed and integrated. The convergence characteristics of both methods were compared as shown in Fig. 13. In the power flow, the *decomposed* method was solved in 33 iterations. The *integrated* method was solved in 14 iterations. In the optimal dispatch, the *decomposed* method was solved in 43 iterations and the *integrated* method was solved in 15 iterations. The comparison shows that the *integrated* method requires less iteration. In a simple example network with 5 nodes, the *decomposed* method was solved in 16 iterations and the *integrated* method was solved in 12 iterations. The comparison shows that the number of the iterations of the *decomposed* method increases with the size of the networks.

7. Conclusions

The combined analysis was used to investigate the integrated electrical and heat energy networks. Two methods for combined analysis were developed to investigate the performance of electricity and heat networks as an integrated whole. Using the combined analysis, an engineering solution was provided to the Barry Island case study. These two methods were the *decomposed* and *integrated* electrical-hydraulic-thermal calculation techniques in the forms of the power flow and simple optimal dispatch. The *integrated* method required fewer iterations and the number of the iterations of the *decomposed* method increased with the size of the networks.

The combined analysis of integrated networks could be expanded by considering local decentralised generation, such as local heat pumps or electric boilers installed at consumers and interconnected to heat networks or the use of micro-CHP. The inclusion of thermal storage in a multi-time simulation is also of interest. Other future work includes integration of more energy vectors and extension of the model to further develop optimisation capabilities to minimise energy losses, costs and carbon emissions in integrated energy networks. In the analysis of a heavily coupled multi-vector energy networks, the integrated electrical-hydraulic-thermal method will play an important role due to its flexibility and capability.

Appendix A

See Table 4.

References

[1] Ekanayake J, Jenkins N, Liyanage K, Wu J, Yokoyama A. Smart grid: technology and applications. Wiley; 2012.

[2] Geidl M, Andersson G. Optimal power flow of multiple energy carriers. IEEE Trans Power Syst 2007;22:145–55.

[3] Flexible energy delivery systems. <http://www.cardiff.ac.uk/ugc/flexible-energy-delivery-system-seminar-series-for-postgraduates-and-researchers> [accessed 25.03.13].

[4] Roskilly AP, Taylor PC, Yan J. Energy storage systems for a low carbon future – in need of an integrated approach. Appl Energy 2015;137:463–6.

[5] Kitapbayev Y, Moriarty J, Mancarella P. Stochastic control and real options valuation of thermal storage-enabled demand response from flexible district energy systems. Appl Energy 2015;137:823–31.

[6] Cho H, Smith AD, Mago P. Combined cooling, heating and power: a review of performance improvement and optimization. Appl Energy 2014;136:168–85.

[7] Chicco G, Mancarella P. Distributed multi-generation: a comprehensive view. Renew Sust Energy Rev 2009;13:535–51.

[8] Mancarella P. MES (multi-energy systems): an overview of concepts and evaluation models. Energy 2014;65:1–17.

[9] Mancarella P, Chicco G. Distributed multi-generation: energy models and analyses. New York: Nova Publisher; 2009.

[10] Yan J. Handbook of clean energy systems, vol. 6. Wiley; 2015.

[11] Lund H, Andersen AN, Østergaard PA, Mathiesen BV, Connolly D. From electricity smart grids to smart energy systems – a market operation based approach and understanding. Energy 2012;42:96–102.

[12] CHPA. Integrated energy: the role of CHP and district heating in our energy future. The Combined Heat and Power Association (CHPA); 2010.

[13] Chaudry M, Jenkins N, Qadrdan M, Wu J. Combined gas and electricity network expansion planning. Appl Energy 2014;113:1171–87.

[14] Seungwon A, Qing L, Gedra TW. Natural gas and electricity optimal power flow. In: Transmission and distribution conference and exposition, IEEE PES, vol. 1; 2003. p. 138–43.

[15] Chaudry M, Jenkins N, Strbac G. Multi-time period combined gas and electricity network optimisation. Electric Power Syst Res 2008;78:1265–79.

[16] Qadrdan M, Chaudry M, Wu J, Jenkins N, Ekanayake J. Impact of a large penetration of wind generation on the GB gas network. Energy Policy 2010;38:5684–95.

[17] Martinez-Mares A, Fuerte-Esquivel CR. A unified gas and power flow analysis in natural gas and electricity coupled networks. IEEE Trans Power Syst 2012;27:2156–66.

[18] Rubio-Barros R, Ojeda-Esteybar D, Vargas A. Energy carrier networks. In: Sorokin A, Rebennack S, Pardalos PM, Iliadis NA, Pereira MVF, editors. Interactions and integrated operational planning handbook of networks in power systems II. Berlin, Heidelberg: Springer; 2012. p. 117–67.

[19] Awad B, Chaudry M, Wu J, Jenkins N. Integrated optimal power flow for electric power and heat in a microgrid. Prague; 2009.

[20] Mancarella P, Chin Kim G, Strbac G. Evaluation of the impact of electric heat pumps and distributed CHP on LV networks. In: PowerTech, 2011 IEEE Trondheim; 2011. p. 1–7.

[21] Navarro-Espinosa A, Mancarella P. Probabilistic modeling and assessment of the impact of electric heat pumps on low voltage distribution networks. Appl Energy 2014;127:249–66.

[22] Blarke MB. Towards an intermittency-friendly energy system: comparing electric boilers and heat pumps in distributed cogeneration. Appl Energy 2012;91:349–65.

[23] Rees MT, Wu J, Jenkins N, Abeysekera M. Carbon constrained design of energy infrastructure for new build schemes. Appl Energy 2014;113:1220–34.

[24] Rees MT, Wu J, Awad B, Ekanayake J, Jenkins N. A modular approach to integrated energy distribution system analysis. In: 17th Power systems computation conference. Stockholm Sweden; 2011.

[25] Rees MT, Wu J, Awad B, Ekanayake J, Jenkins N. A total energy approach to integrated community infrastructure design. In: Power and energy society general meeting, 2011. IEEE; 2011.

[26] Mancarella P. Cogeneration systems with electric heat pumps: energy-shifting properties and equivalent plant modelling. Energy Convers Manage 2009;50:1991–9.

[27] Weedy BM, Cory BJ, Jenkins N, Ekanayake JB, Strbac G. Electric power systems. 5th ed. Wiley; 2012.

[28] Grainger JJ, Stevenson WD. Power system analysis. New York: McGraw-Hill; 1994.

[29] Zhao H. Analysis, modelling and operational optimization of district heating systems. PhD Thesis. Technical University of Denmark; 1995.

[30] Fedorov M. Parallel implementation of a steady state thermal and hydraulic analysis of pipe networks in OpenMP. In: Wyrzykowski R, Dongarra J, Karczewski K, Wasniewski J, editors. Parallel processing and applied mathematics, vol. 6068. Berlin/Heidelberg: Springer; 2010. p. 360–9.

[31] Siemens. PSS sincal 7.0 heating manual; 2010.

[32] Larock BE, Jeppson RW, Watters GZ. Hydraulics of pipeline systems. CRC; 2000.

[33] Osiadacz A. Simulation and analysis of gas networks. Gulf Pub. Co.; 1987.

[34] Liu X. Combined analysis of electricity and heat networks. PhD Thesis. Cardiff University; 2013.

[35] Steer KCB, Wirth A, Halgamuge SK. Control period selection for improved operating performance in district heating networks. Energy Build 2011;43:605–13.

[36] 7-Technologies. TERMIS Help Manual; 2009.

[37] Benonysson A. Dynamic modelling and operational optimization of district heating systems. PhD Thesis. Laboratory of Heating and Air Conditioning. Technical University of Denmark; 1991.

[38] Byun J, Choi Y, Shin J, Park M, Kwak D. Study on the development of an optimal heat supply control algorithm for group energy apartment buildings according to the variation of outdoor air temperature. Energies 2012;5:1686–704.

[39] Bøhm B, Danig PO. Monitoring the energy consumption in a district heated apartment building in Copenhagen, with specific interest in the thermodynamic performance. Energy Build 2004;36:229–36.

[40] Saarinen L. Modelling and control of a district heating system. Uppsala University, Department of Information Technology; 2008. p. 12.

[41] Bøhm B, Ha S, Kim W, Kim B, Koljonen T, Larsen H, et al. Simple models for operational optimisation: department of mechanical engineering. Technical University of Denmark; 2002.

[42] Coulson JM, Richardson JF, Sinnott RK. Coulson & Richardson's chemical engineering. Fluid flow, heat transfer & mass transfer, vol. 1. Butterworth Heinemann Ltd; 1999.

[43] Ben Hassine I, Eicker U. Impact of load structure variation and solar thermal energy integration on an existing district heating network. Appl Therm Eng 2013;50:1437–46.

[44] Seugwon A. Natural gas and electricity optimal power flow. PhD thesis. Oklahoma State University; 2004.

[45] CHPQA. GUIDANCE NOTE 28: the determination of Z ratio. <https://www.chpqa.com/guidance_notes/GUIDANCE_NOTE_28.pdf> [accessed 01.06.13].

[46] Glover JD, Sarma MS, Overbye TJ. Power systems analysis & design. Thomson; 2008.

[47] Ingram S, Probert S, Jackson K. The impact of small scale embedded generation upon the operating parameters of distribution networks. DTi New and Renewable Energy Program, K/EL/00303/04/01; 2003.

[48] Goldstein L. Gas-fired distributed energy resource technology characterizations: national renewable energy laboratory; 2003.

[49] EPA. Catalog of CHP Technologies: U.S. Environmental Protection Agency (EPA) Combined Heat and Power Partnership; 2008.

[50] MATPOWER. <http://www.pserc.cornell.edu/matpower/> [accessed 03.04.10].